Experimental characterization of photon-number noise in Rarity-Tapster-Loudon-type interferometers

Vojtěch Trávníček,[1,*] Karol Bartkiewicz,[1,2,†] Antonín Černoch,[1,‡] and Karel Lemr[1,§]
[1]*RCPTM, Joint Laboratory of Optics of Palacký University and Institute of Physics of Czech Academy of Sciences, 17. Listopadu 12, 771 46 Olomouc, Czech Republic*
[2]*Faculty of Physics, Adam Mickiewicz University, PL-61-614 Poznań, Poland*
(Received 18 April 2017; published 22 August 2017)

In this paper, we develop a simple model describing inherent photon-number noise in Rarity-Tapster-Loudon-type interferometers. This noise is caused by generating photon pairs in the process of spontaneous parametric down-conversion and adding a third photon by attenuating the fundamental laser mode to the single-photon level. We experimentally verify our model and present resulting signal-to-noise ratios as well as obtained three-photon generation rates as functions of various setup parameters. Subsequently we evaluate the impact of this particular source of noise on quantum teleportation which is a key quantum information protocol using this interferometric configuration.

DOI: 10.1103/PhysRevA.96.023847

I. INTRODUCTION

Quantum information processing (QIP) is a modern and perspective research discipline of information science [1–3]. One of the platforms suitable for QIP are discrete photons manipulated using linear optics [4]. This platform is particularly promising for quantum communications, because of fast and relatively noiseless propagation of individual photons through open space or in fibers [5,6].

Quantum teleportation [7,8] is a key ingredient for many quantum information protocols such as entanglement swapping [9], quantum relays [10] or teleportation-based quantum computing [11]. On the platform of linear optics, quantum teleportation is usually achieved in the so-called Rarity-Tapster-Loudon interferometer [12] (shown in Fig. 1). In this interferometer, one photon from an entangled pair gets overlapped on a balanced beam splitter with an independent photon [4]. The output ports of the beam splitter are then subjected to suitable Bell-state projection. Multiphoton interferometers have also a number of potential applications that go beyond quantum teleportation (for a review see Ref. [13]). For example, they can also be used for engineering of cluster states [14].

Single-photon sources used in experimental quantum information processing today are, however, imperfect and the number of photons generated per pulse is random, given by the state's photopulse statistics (e.g., Bose-Einstein, Poisson). While vacuum states can be filtered out by suitable post-selection, higher photon-number contributions cannot always be recognized [15,16].

The cornerstone of linear-optical quantum information processing is the phenomenon of two-photon interference (Hong-Ou-Mandel bunching) [17]. In 1988, Ou and Mandel predicted that visibility of two-photon bunching with classical beams is limited to 50% due to their photon-number statistics [18]. This research was further generalized to interaction between classical beam and ideal single-photon source [12]. Subsequently, experimentalists have managed to approach the visibility limit in Rarity-Tapster-Loudon interferometers by optimizing spectral properties of interacting beams [19–21]. The photon-number noise in a Hong-Ou-Mandel interferometer fed by a source of photons generated in the process of spontaneous parametric down-conversion (SPDC) was analyzed in Ref. [22]. Independently, several research groups have investigated two-photon bunching between two heralded single-photon sources [23–25]. Suitable modification of the signal generation rate with respect to the ancilla generation rate can considerably improve teleportation fidelity in a scheme with two SPDC sources [26]. Visibility of observed interference patterns depends on various properties of incident photons (polarization, frequency, and spatial mode overlap), on stability of their arrival time (arrival-time jitter), and finally on the noise consisting of unwanted additional photons. The properties of interfering photons strongly depend on the particular choice of the experimental components. The arrival-time jitter is then given by the choice of pumping pulse width and SPDC media length. Here, we investigate the influence of photon-number noise of photon sources on the maximal attainable visibility of the observed interference pattern. The maximal interference visibility and consequently the fidelity of implemented multiphoton QIP protocols can be calculated knowing the amount of the photon-number noise.

In this paper, we present a simple and practical model describing inherent photon-number noise in Rarity-Tapster-Loudon-type interferometers based on a SPDC sources and attenuated coherent state. These are currently predominant photon sources in experimental linear-optical QIP [5,27–32]. We have experimentally tested validity of our model and established both theoretical and experimental relations between photon-number noise and various setup parameters. To our best knowledge no article providing such an analysis has yet been published. The influence of transmission noise on the fidelity and security of quantum teleportation of qubits was analyzed in Ref. [33]. The photon-number noise does not originate from experimental imperfections but is rather an intrinsic property of a photon source (i.e., its photon-number

*vojtech.travnicek01@upol.cz
†bartkiewicz@jointlab.upol.cz
‡antonin.cernoch@upol.cz
§k.lemr@upol.cz

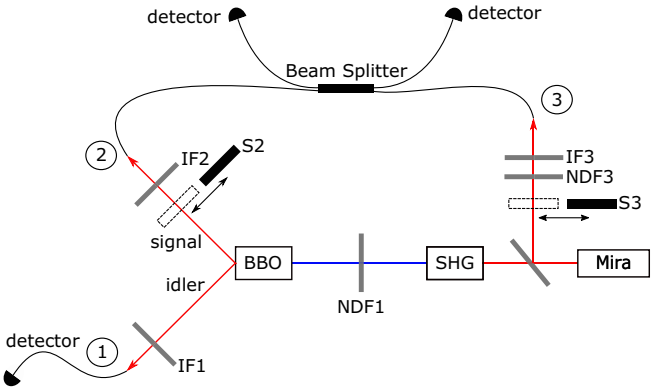

FIG. 1. Setup of the experiment. (1) Idler mode, (2) signal mode, (3) attenuated fundamental laser mode, [IF(1-3)] interference filters (3 nm in FWHM), [NDF(1,3)] neutral density filter, [S(2,3)] shutters, (SHG) second harmonics generation, (Mira) Ti-sapphire fs laser (central wavelength of 826 nm, FWHM of 11 nm), (BBO) a β-BaB_2O_4 crystal for SPDC.

statistics). Its irremovibility even further stresses out the significance of this investigation. One can evaluate the level of the photon-number noise independently of the visibility of the two-photon interference. This makes such analysis free of potential uncertainties arising from interference imperfections.

The paper is organized as follows: In Sec. II we develop a theoretical model describing dependency of signal-to-noise ratio on the main parameters of the experimental setup. In Sec. III we present experimental data verifying our model. In Sec. IV we investigate the impact of the photon-number noise on teleportation fidelity. We conclude in Sec. V.

II. THEORETICAL MODEL

Here, we assume that the pairs of photons are generated in the process of degenerate parametric down-conversion. The generated optical fields are not strictly monochromatic, but for each wavelength from their spectrum the following reasoning holds. Let us denote $|\psi_s\rangle$ the state of signal and idler modes of the SPDC generated photons (Nos. 1 and 2) and $|\alpha\rangle$ the coherent state of the attenuated fundamental laser mode (No. 3). We start with the Hamiltonian for the SPDC process [34] in the form of

$$\hat{H} = \hbar\omega(\hat{a}_1^\dagger\hat{a}_1 + \hat{a}_2^\dagger\hat{a}_2) + \hbar\omega_p\hat{a}_3^\dagger\hat{a}_3 + i\hbar\chi^{(2)}(\hat{a}_1\hat{a}_2\hat{a}_3^\dagger - \hat{a}_1^\dagger\hat{a}_2^\dagger\hat{a}_3), \quad (1)$$

where $\hat{a}_1^\dagger$, $\hat{a}_2^\dagger$ are creation operators of the idler and signal photon modes of equal frequency ω, respectively, and $\hat{a}_3^\dagger$ is a mode of frequency doubled laser beam. The pump frequency is equal to the frequency of the generated signal and idler photons, i.e., $\omega_p = 2\omega$. If the pump amplitude α_p is large, we can apply the parametric approximation, which results in the following Hamiltonian:

$$\hat{H} = \hbar\omega(\hat{a}_1^\dagger\hat{a}_1 + \hat{a}_2^\dagger\hat{a}_2) + i\hbar\chi^{(2)}(\alpha_p^*\hat{a}_1\hat{a}_2e^{-i2\omega t} - \alpha_p\hat{a}_1^\dagger\hat{a}_2^\dagger e^{i2\omega t}), \quad (2)$$

where we have neglected the constant terms. It turns out that this Hamiltonian, due to the special relations between frequencies of the pump, signal, and idler modes, can be rewritten in a time-independent form in the interaction picture as

$$\hat{H}_{\mathrm{SPDC}} = i\hbar\chi^{(2)}(\alpha_p^*\hat{a}_1\hat{a}_2 - \alpha_p\hat{a}_1^\dagger\hat{a}_2^\dagger) = \gamma\alpha_p\hat{a}_1^\dagger\hat{a}_2^\dagger + \mathrm{H.c.}, \quad (3)$$

where $\gamma \ll 1$ is an interaction constant. The corresponding evolution operator is then of the form of

$$\hat{U} = \exp\left(-\frac{it}{\hbar}\hat{H}_{\mathrm{SPDC}}\right). \quad (4)$$

The state of the signal and idler modes is obtained by applying the $\hat{U}$ operator to the initial vacuum state,

$$|\psi_s\rangle \propto |00\rangle + \frac{it}{\hbar}\gamma\alpha_p|11\rangle + \frac{(it\gamma\alpha_p)^2}{2\hbar^2}|22\rangle + \cdots \quad (5)$$

We can express this state as

$$|\psi_s\rangle \propto |00\rangle + \kappa|11\rangle + \frac{\kappa^2}{2}|22\rangle, \quad (6)$$

for $|\kappa| \ll 1$ and

$$\kappa = \frac{it}{\hbar}\gamma\alpha_p. \quad (7)$$

The term $|00\rangle$ in Eq. (6), can be omitted because the first photon works as a herald which means that if it does not get detected the measurement will not succeed. This is under the assumption of negligible dark counts. Furthermore, we have to take into account probability of coupling of the photons from SPDC into optical fibers. Let us denote t_1 and t_2 the amplitude coupling efficiency of idler and signal modes, respectively. The state of the first and second photon then reads

$$|\psi_s\rangle \propto 2\kappa t_1t_2|11\rangle + 2\kappa t_1\sqrt{1-t_2^2}|10\rangle + \kappa^2t_1\sqrt{1-t_1^2t_2^2}|12\rangle + \kappa^2t_1^2t_2^2|22\rangle, \quad (8)$$

where again we have excluded the terms corresponding to the first mode being in a vacuum state. Moreover, the last term in Eq. (8) can be neglected with respect to the third term since in typical experimental setups $t_{1,2} \ll 1$.

Next, we can express the coherent state of the attenuated fundamental laser mode of the same wavelength as the generated photon pairs in the Fock basis and limit the expansion to the first N terms,

$$|\alpha\rangle \approx \sum_{n=0}^{N}\frac{\alpha^n}{\sqrt{n!}}|n\rangle. \quad (9)$$

Any filtering or coupling efficiency does not change the nature of the attenuated laser mode which remains in a coherent state with amplitude α already including all possible losses. Thus we do not need to consider its coupling efficiency like in the SPDC modes.

If the source were to be perfect, there should be precisely one photon in each of the three modes. Simultaneous detection of these photons corresponds to genuine coincidences denoted CC_g. In reality, SPDC-based sources yield also higher-photon-number contributions. On the beam splitter, these photons may

split leading to three-photon detection even if there were no photons in the attenuated laser mode [see the third term in Eq. (8)]. These detections denoted CC_s contribute to added noise. Similar source of noise are higher photon-number contributions from the fundamental laser mode that again can split on the beam splitter resulting in parasitic detections CC_f. Using Eqs. (8) and (9) for $N = 3$, we can identify the generation probabilities of the genuine coincidences as well as of the two parasitic contributions,

$$CC_g \propto |\kappa|^2|\alpha|^2 t_1^2 t_2^2, \tag{10}$$

$$CC_s \propto t_1^2 t_2^4 \frac{|\kappa|^4}{4}, \tag{11}$$

$$CC_f \propto |\kappa|^2 t_1^2 \left(\frac{|\alpha|^4}{2} + \frac{|\alpha|^6}{6}\right). \tag{12}$$

Note that in Eq. (11), we have assumed $1 - t_1^2 \approx 1$ and in Eq. (12) $1 - t_2^2 \approx 1$. These approximations are valid especially when one considers a linear-optical setup fed by the source which strongly diminishes the transmissivity due to technological losses (back-scattering, fiber coupling, etc.).

The goal now is to maximize the signal-to-noise ratio defined as

$$\mathrm{SNR} \equiv \frac{CC_g}{CC_s + CC_f} = \frac{12|\alpha|^2 t_2^2}{3|\kappa|^2 t_2^4 + 6|\alpha|^4 + 2|\alpha|^6}. \tag{13}$$

In a typical setup as depicted in Fig. 1, there are two parameters that can easily be tuned: (i) amplitude of the attenuated fundamental laser mode α and (ii) SPDC pumping amplitude α_p. In subsequent analysis, we investigate the dependency of SNR on these two parameters.

First, we look at SNR as a function of α, which translates to the observed ratio R between coincidence rates CC_f and CC_s,

$$R \equiv \frac{CC_f}{CC_s} = \frac{2|\alpha|^4}{|\kappa|^2 t_2^4} + \frac{2|\alpha|^6}{3|\kappa|^2 t_2^4} \approx \frac{2|\alpha|^4}{|\kappa|^2 t_2^4}. \tag{14}$$

We have omitted the second expansion term from CC_f because for typical levels of attenuation to the single-photon level $|\alpha| \ll 1$. The signal-to-noise ratio can now be approximated as a function of the parameter R,

$$\mathrm{SNR} \approx \frac{2\sqrt{2R}}{|\kappa|(R+1)}. \tag{15}$$

One can now find the optimal value of R by searching for maximum of this function. When $|\alpha| \ll 1$ holds, the optimal value of R is 1. For larger values of $|\alpha|$ the optimal R shifts to slightly lower values because the approximation in Eq. (14) no longer applies. In an experiment, one should thus seek to balance the false coincidence rates from SPDC and from the attenuated fundamental mode.

In the subsequent analysis, we assume that $|\alpha| \ll 1$ holds and fix the parameter R at its optimal value of 1. Equation (15) then simplifies into the form,

$$\mathrm{SNR} = \frac{\sqrt{2}}{|\kappa|}, \tag{16}$$

which can, with the help of Eqs. (10) and (14), be expressed in terms of the genuine coincidence rate CC_g,

$$\mathrm{SNR} \propto \sqrt[3]{\frac{16 t_1^2 t_2^4}{CC_g}}. \tag{17}$$

One can now make two important conclusions towards the performance of the interferometer. First, the SNR can only be increased by decreasing the value of $|\kappa|$ which means by lowering the SPDC pumping strength $|\alpha_P|$. Secondly, the obtained coincidence rate depends on the coupling efficiency of the signal and idler SPDC modes. Especially, it scales with the fourth power of the amplitude transmissivity of the signal mode (or second power of intensity transmissivity). For any given pumping strength, one can improve the overall coincidence rate by improving the coupling efficiencies. The SNR, however, cannot be improved by this adjustment.

III. EXPERIMENTAL IMPLEMENTATION

We have subjected our model and the resulting conclusions to an experimental test. Our experimental setup is depicted in Fig. 1. The attenuated fundamental laser mode (mode No. 3) is obtained by splitting a small portion from the femtosecond pumping laser beam (Coherent Mira at 826 nm). It then passes through a neutral density filter (NDF3) and 3-nm-wide interference filter (IF3) before being coupled into single-mode fiber.

The main laser beam enters the second harmonics generation unit (SHG), where its wavelength becomes 413 nm. The beam then passes through a neutral density filter (NDF1) and enters a Type I cut BBO crystal (0.64-mm thick) which due to SPDC generates idler and signal photons (Nos. 1 and 2), respectively. The photons in signal mode then pass through a 3-nm-wide interference filter (IF2). The photons in idler mode pass through a 10-nm-wide interference filter (IF1). The two SPDC modes are then coupled into single-mode fibers, and the idler mode is directly led to a single-photon detector unlike modes 2 and 3 that are mixed in a 50:50 fiber coupler before being detected. The avalanche photodiode detectors with suitable electronics record threefold coincidence detections. The coincidence detection window was set to 5 ns, less than the laser repetition period of approximately 12.5 ns. We set the temporal displacement between photons 2 and 3, so they do not overlap in the fiber coupler. Thus we prevent the effect of two-photon interference.

In our experiment, we performed all the testing measurements in three steps: (i) with the shutters S2 and S3 open we detect all threefold coincidences CC_a which include CC_g and parasitic contributions from signal and attenuated fundamental laser mode CC_s and CC_f,

$$CC_a = CC_g + CC_f + CC_s. \tag{18}$$

(ii) Then we close shutter S3 and obtain threefold coincidences only if there is more than one photon in signal mode, thus we measure parasitic coincidence rate CC_s. (iii) Finally we close shutter S2, open S3, and therefore obtain threefold coincidences only if there is more than one photon in the attenuated fundamental laser mode—parasitic coincidence rate CC_f. Note that CC_g is obtained from Eq. (18) simply

TABLE I. Experimentally observed data and their respective errors when investigating the dependence of SNR on the parameter R.

SNR (dB)	Parameter R
-6.222 ± 0.740	0.013 ± 0.004
-4.440 ± 0.432	0.030 ± 0.004
-3.010 ± 0.440	0.040 ± 0.006
-1.105 ± 0.388	0.080 ± 0.008
-0.530 ± 0.442	0.340 ± 0.021
-0.086 ± 0.392	1.130 ± 0.052
-2.201 ± 0.241	1.510 ± 0.057
-3.502 ± 0.667	3.290 ± 0.290
-6.434 ± 0.727	7.180 ± 0.680

by subtracting CC_f and CC_s from CC_a. Each step took about 100 s and the entire three-step procedure was repeated multiple times, thus we have avoided a bias caused by longterm laser power fluctuations.

First, we have experimentally verified the dependence of SNR on α, hence as a function of R [see Eq. (15)]. The experiment consisted of measuring the coincidence rates for various values of R using the above-mentioned three steps. The parameter R was changed by modifying the transmissivity of NDF3. Experimentally obtained values are summarized in Table I and visualized in Fig. 2 together with the theoretical fit based on Eq. (15). The dashed line shows a fit in which we limited the expansion in Eq. (9) to $N = 2$, however, it turns out that the model is not accurate enough for $R \to 10$ (see Fig. 2). With growing contribution of parasitic coincidences from the attenuated fundamental laser mode CC_f, and thus also growing ratio R, higher terms in Eq. (9) can no longer be neglected and the approximation in Eq. (14) no longer holds. The solid line which represents a model where we used expansion up to $N = 3$, is accurate enough throughout the entire measured range of R. We went a step further and expanded our model (represented in Fig. 2 by the dash-dot line) to include terms up to $N = 4$ in the expansion. There is a slight but unsubstantial improvement to the previous case and thus we find the four-term expansion to be the optimum compromise between accuracy and complexity. To simplify the following experiments, we have set the attenuated laser

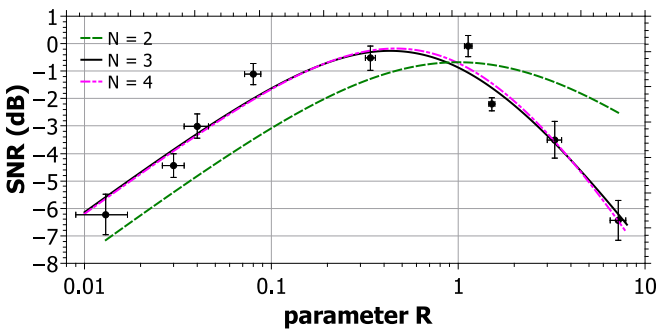

FIG. 2. Dependence of SNR on parameter R. Points visualize experimentally observed results. Lines correspond to various levels of expansion in Eq. (9): to 2 (green dashed line), 3 (black solid line), and 4 (magenta dashed-dot line) terms.

TABLE II. Experimentally observed data and their respective errors when investigating the dependence of SNR on the CC_g and CC_g on the α_p.

SNR (dB)	CC_g per 100 s	$P_p \propto \lvert\alpha_p\rvert^2$ (mW)
9.91 ± 1.27	2.91 ± 0.11	13 ± 2
7.50 ± 0.79	7.23 ± 0.22	25 ± 2
6.23 ± 0.71	19.88 ± 0.61	50 ± 2
5.17 ± 0.56	51.59 ± 1.38	104 ± 3
3.33 ± 0.58	135.28 ± 4.39	190 ± 3

beam power so that the approximation in Eq. (14) holds. This means setting $R \in [0.2; 1]$ which also coincides with the SNR maximum.

As the next test, we have measured the dependence of SNR on the pumping amplitude α_p, which also translates into the dependence of SNR on the genuine coincidence rate CC_g [see Eqs. (16) and (17)]. We maintained the ratio R close to its optimum discovered in the previous test ($R \approx 0.35 \pm 0.04$) and were changing α_p by changing transmissivity of NDF1. So for every measured value of SNR, we have adjusted both the NDF1 (influencing α_p) and NDF3 (to maintain constant R). The measurement procedure was also realized in the previously mentioned three acquisition steps. Experimentally obtained values are summarized in Table II and visualized in Fig. 3 together with a theoretical fit based on Eq. (16). Figure 3 proves that our four-term model matches well the experimental data. We have also investigated dependence of CC_g on pumping power P_p which is proportional to pumping amplitude $|\alpha_p|^2$.

The final two tests of our model involved verifying the dependence of genuine coincidence rate CC_g on the coupling efficiencies (i) t_1 and (ii) t_2 as predicted in Eq. (17). During each of the two tests, the parameter R and the pumping power were kept constant resulting in constant SNR. During the first test the value of SNR was (4.7 ± 1.6)dB. In the second test the SNR was (5.0 ± 1.3)dB. In order to test the dependence on idler and signal mode transmissivities t_1 and t_2, we have acquired the coincidences in the usual three steps for various

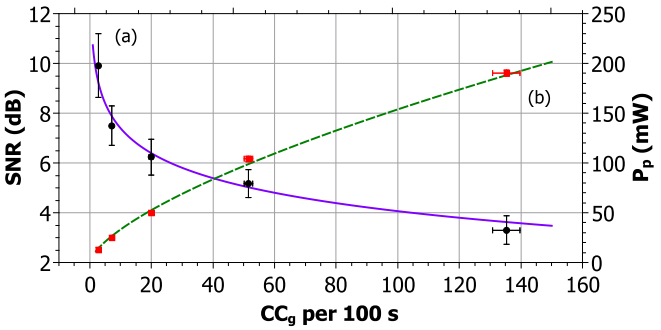

FIG. 3. (a) Dependence of SNR on genuine coincidence rate CC_g. Points visualize experimentally observed results; the solid blue line depicts fitted experimental data with theoretical dependence based on Eq. (16). (b) Dependence of CC_g on P_p. The dashed green line depicts fitted experimental data with theoretical dependence based on Eq. (10).

TABLE III. Experimentally observed data and their respective errors when investigating the dependence of CC_g on the attenuation factors A_1 and A_2.

Idler attenuation (t_1)		Signal attenuation (t_2)	
A_1	CC_g per 100 s	A_2	CC_g per 100 s
1.0	41.2 ± 3.2	1.0	44.8 ± 2.5
1.4	27.2 ± 1.7	1.3	22.2 ± 1.5
2.0	19.0 ± 1.7	1.9	10.0 ± 1.0
2.7	14.3 ± 1.8	2.8	6.2 ± 1.0
4.0	10.0 ± 1.7	3.8	2.3 ± 0.3

levels of attenuation by closing a diaphragm on the idler and signal mode fiber couplers, respectively. When the signal mode attenuation was set, the NDF3 in the attenuated fundamental laser mode was readjusted to maintain a constant R. This was not necessary when closing the idler mode diaphragm. For better readability of our results, we introduce the idler and signal mode intensity attenuation factors A_1 and A_2 so that the modes' transmissivities become $t_j^2 \to t_j^2/A_j$ for $j = 1,2$. Experimentally observed values are summarized in Table III and visualized in Fig. 4. Figure 4 demonstrates that with constant SNR CC_g depends on modes' transmissivities t_1^2 and t_2^2 as functions $\frac{1}{x}$ and $\frac{1}{x^2}$, respectively, as predicted in Eq. (17).

IV. IMPACT OF THE NOISE ON TELEPORTATION FIDELITY

We now investigate the impact of the above analyzed noise on quantum teleportation. Since quantum teleportation is a key ingredient in many quantum information protocols, it is essential to assess the influence of inherent noise of various photon sources on its performance. In quantum circuits, including teleportation, one often uses fidelity as a measure of the circuits' quality. Assuming a pure input qubit state $|\psi\rangle_{\text{in}}$ and the resulting teleported state $\hat{\rho}_{\text{out}}$, fidelity can be calculated using the formula

$$F = |\langle\psi_{\text{in}}|\hat{\rho}|\psi_{\text{in}}\rangle|. \tag{19}$$

Note that when teleportation is replaced by the classical "measure and recreate" protocol, the fidelity cannot exceed its

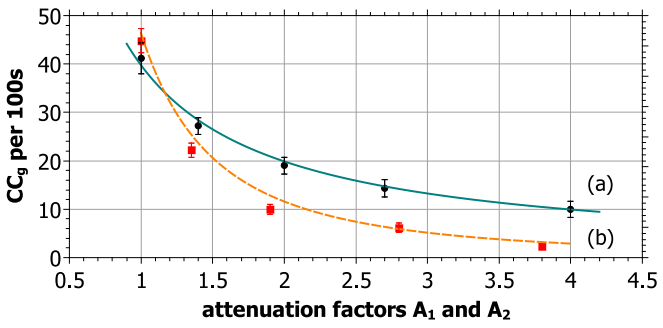

FIG. 4. Dependence of CC_g on attenuation factors (a) A_1, solid green line, and (b) A_2, dashed orange line. Points visualize experimentally observed results; lines depict fitted experimental data with theoretical fit based on Eq. (17).

TABLE IV. Calculated data and their respective errors when investigating the dependence of average fidelity F on the SNR.

Fidelity F	Fidelity uncertainty interval	SNR (dB)
0.96	⟨0.93,0.98⟩	9.91 ± 1.27
0.94	⟨0.90,0.96⟩	7.50 ± 0.79
0.92	⟨0.86,0.95⟩	6.23 ± 0.71
0.89	⟨0.85,0.91⟩	5.17 ± 0.56
0.85	⟨0.83,0.86⟩	3.29 ± 0.58

classical limit of $\frac{2}{3}$ [35]. Even though it is impossible to reach perfect fidelity $F = 1$ in realistic conditions, one still targets to maximize its value.

In our analysis we have calculated the dependence of average fidelity $\langle F\rangle$ on the signal-to-noise ratio (SNR). If we fix the parameter R to its optimum value ($R \approx 0.35$), fidelity $\langle F\rangle$ is then a function that depends on CC_g and only one of the CC_s or CC_f since these two are bound by fixed parameter R. As a result the fidelity is a function of SNR. We have calculated the average fidelity using the formula,

$$\langle F\rangle = \frac{P_{CC_g}F_g + P_{CC_s}F_s + P_{CC_f}F_f}{P_{CC_g} + P_{CC_s} + P_{CC_s}}, \tag{20}$$

where

$$P_{CC_g} = \frac{CC_g}{4f}, \quad P_{CC_s} = \frac{CC_s}{4f}, \quad P_{CC_f} = \frac{CC_f}{4f} \tag{21}$$

are the probabilities of the coincidence events. f stands for the repetition rate of the pumping laser and F_g, F_s, F_f are the teleportation fidelities if the coincidence CC_g, CC_s or CC_f occur, respectively. The value of teleportation fidelity F_g equals 1 because there is one photon in each mode so the teleportation succeeds perfectly, at least in principle. On the other hand, the teleportation fidelities F_s and F_f both have values of $\frac{1}{2}$—the first one because the two photons in signal mode are randomly projected onto Bell states uncorrelated with the teleported photon which is missing, and the latter one because the two photons in the attenuated laser mode are not correlated with the idler mode which is thus in a mixed state.

Calculated values are summarized in Table IV and visualized in Fig. 5. We observe that the average fidelity drops only slightly with decreasing SNR, so the average fidelity is above 80% for SNR around 3 dB. This analysis provides the limit of attainable teleportation fidelity with the photon-number noise as the only source of decreased interference visibility. It does not take into account other experimental imperfections such as two-photon overlap, polarization adjustments, etc. All the above-mentioned sources of noise combined can make the protocol fail because of its insufficient fidelity. When implementing a quantum teleportation-based scheme, one can use our analysis to evaluate the maximal attainable fidelity and consider available margin for error arising from other experimental imperfections.

The fidelity uncertainty intervals were calculated using a Monte Carlo simulation based on Poisson distribution of detected coincidences.

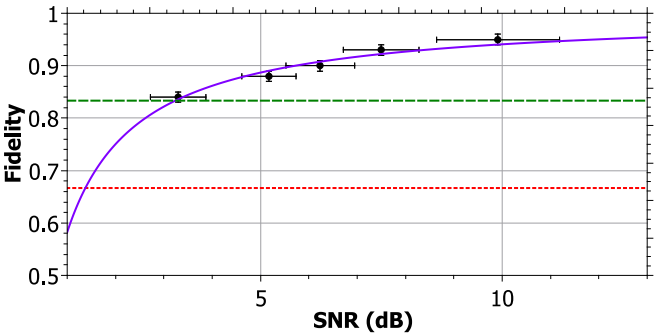

FIG. 5. Dependence of average fidelity $\langle F \rangle$ on SNR. Points visualize calculated results from experimentally observed SNRs. The solid blue line corresponds to our theoretical model, the dotted red line is the classical protocol limit ($F = 2/3$) [35], and the dashed green line indicates the secure teleportation, i.e., $F = 5/6$ cloning threshold; see [33].

V. CONCLUSIONS

In conclusion, we have shown that our model fits the experimental data very well. We have demonstrated the role of the ratio R between the SPDC-based and attenuated fundamental-based false coincidences. We have also confirmed its optimal value being close to 1 depending on the pumping strength. In the next step, we have verified that SNR (when optimal R) can only be increased by decreasing the SPDC pumping strength. Our data fit well both the SNR as a function of the genuine coincidence rate and also the predicted coincidence rate as a function of pumping strength. Finally, we have successfully tested the genuine coincidence rates as functions of coupling efficiencies while maintaining constant SNR. Our model and the obtained conclusions drawn from it can be useful for experimentalists when constructing a similar three-photon source and using it for teleportationlike protocols. With respect to that, we have made a prediction of the impact of this noise to teleportation fidelity. While fidelity drops smoothly with decreasing SNR, in conjunction with other experimental imperfections it may fall below the classical threshold or at least below the threshold of secure teleportation.

ACKNOWLEDGMENTS

The authors thank Jan Soubusta for a helpful discussion regarding the paper. The authors acknowledge financial support from the Czech Science Foundation under Project No. 17-10003S. K.L. and K.B. also acknowledge financial support from the Polish National Science Centre under Grant No. DEC-2013/11/D/ST2/02638. The authors also acknowledge Project No. LO1305 of the Ministry of Education, Youth and Sports of the Czech Republic for financing the infrastructure of their workplace and V.T. also acknowledges the Palacky University, internal Grant No. IGA-PrF-2017-005.

[1] G. Alber, T. Beth, M. Horodecki, P. Horodecki, R. Horodecki, M. Rötteler, H. Weinfurter, R. Werner, and A. Zeilinger, *Quantum Information* (Springer, Berlin, 2001).

[2] M. Nielsen and I. Chuang, *Quantum Computation and Quantum Information* (Cambridge University Press, Cambridge, 2002).

[3] D. Bowmeester, A. Ekert, and A. Zeilinger, *The Physics of Quantum Information* (Springer, Berlin, 2000).

[4] P. Kok, W. J. Munro, K. Nemoto, T. C. Ralph, J. P. Dowling, and G. J. Milburn, Linear optical quantum computing with photonic qubits, Rev. Mod. Phys. **79**, 135 (2007).

[5] X.-S. Ma, T. Herbst, and T. Sheidl, Quantum teleportation over 143 kilometres using active feed-forward, Nature (London) **489**, (2012).

[6] Q.-C. Sun, Y.-L. Mao, S.-J. Chen, W. Zhang, Y.-F. Jiang, Y.-B. Zhang, W.-J. Zhang, S. Miki, T. Yamashita, H. Terai, X. Jiang, T.-Y. Chen, L.-X. You, X.-F. Chen, Z. Wang, J.-Y. Fan, Q. Zhang, and J.-W. Pan, Quantum teleportation with independent sources and prior entanglement distribution over a network, Nat. Photon. **10**, 671 (2016).

[7] C. H. Bennett, G. Brassard, C. Crépeau, R. Jozsa, A. Peres, and W. K. Wootters, Teleporting an Unknown Quantum State via Dual Classical and Einstein- Podolsky-Rosen Channels, Phys. Rev. Lett. **70**, 1895 (1993).

[8] D. Bouwmeester, J. Pan, K. Mattle, M. Eibl, H. Weinfurter, and A. Zeilinger, Experimental quantum teleportation, Nature (London) **390**, 575 (1997).

[9] X.-s. Ma, S. Zotter, J. Kofler, R. Ursin, T. Jennewein, Č. Brukner, and A. Zeilinger, Experimental delayed-choice entanglement swapping, Nat. Phys. **8**, 479 (2012).

[10] W. Tittel, J. Brendel, B. Gisin, T. Herzog, H. Zbinden, and N. Gisin, Experimental demonstration of quantum correlations over more than 10 km, Phys. Rev. A **57**, 3229 (1998).

[11] D. Gottesman and I. L. Chuang, Demonstrating the viability of universal quantum computation using teleportation and single-qubit operations, Nature (London) **402**, 390 (1999).

[12] J. G. Rarity, P. R. Tapster, and R. Loudon, Non-classical interference between independent sources, J. Opt. B **7**, S171 (2005).

[13] J.-W. Pan, Z.-B. Chen, C.-Y. Lu, H. Weinfurter, A. Zeilinger, and M. Żukowski, Multiphoton entanglement and interferometry, Rev. Mod. Phys. **84**, 777 (2012).

[14] T. Tashima, T. Wakatsuki, Ş. K. Özdemir, T. Yamamoto, M. Koashi, and N. Imoto, Local Transformation of Two Einstein-Podolsky-Rosen Photon Pairs into a Three-Photon W State, Phys. Rev. Lett. **102**, 130502 (2009).

[15] B. Lounis and M. Orrit, Single-photon sources, Rep. Prog. Phys. **68**, 0034 (2005).

[16] S. Scheel, Single-photon sources—an introduction, J. Mod. Opt. **56**, 141 (2009).

[17] C. K. Hong, Z. Y. Ou, and L. Mandel, Measerement of Subpicosecond Time Intervals between Two Photons by Interference, Phys. Rev. Lett. **59**, 2044 (1987).

[18] Z. Y. Ou and L. Mandel, Observation of Spectral Quantum Beating with Separated Photodetectors, Phys. Rev. Lett. **61**, 54 (1988).

[19] K. Laiho, K. N. Cassemiro, and Ch. Silberhorn, Producing high fidelity single photons with optimal brightness via waveg-

uided parametric down-conversion, Opt. Express **17**, 22823 (2009).

[20] R.-B. Jin, J. Zhang, R. Shimizu, N. Matsuda, Y. Mitsumori, H. Kosaka, and K. Edamatsu, High-visibility nonclassical interference between intrinsically pure heralded single photons and photons from a weak coherent field, Phys. Rev. A **83**, 031805(R) (2011).

[21] G. Harder, V. Ansari, B. Brecht, T. Dirmeier, Ch. Marquardt, and Ch. Silberhorn, An optimized photon pair source for quantum circuits, Opt. Express **21**, 13975 (2013).

[22] O. Cosme, S. Pádua, F. A. Bovino, A. Mazzei, F. Sciarrino, and F. De Martini, Hong-Ou-Mandel interferometer with one and two photon pairs, Phys. Rev. A **77**, 053822 (2008).

[23] N. Bruno, A. Martin, and R. T. Thew, Generation of tunable wavelength coherent states and heralded single photons for quantum optics applications, Opt. Commun. **327**, 17 (2014).

[24] R.-Bo. Jin, T. Gerrits, M. Fujiwara, R. Wakabayashi, T. Yamashita, S. Miki, H. Terai, R. Shimizu, M. Takeoka, and M. Sasaki, Spectrally resolved Hong-Ou-Mandel interference between independent photon sources, Opt. Express **23**, 28836 (2015).

[25] M. M. Weston, H. M. Chrzanowski, S. Wollmann, A. Boston, J. Ho, L. K. Shalm, V. B. Verma, M. S. Allman, S. W. Nam, R. B. Patel, S. Slussarenko, and G. J. Pryde, Efficient and pure femtosecond-pulse-length source of polarization-entangled photons, Opt. Express **24**, 10869 (2016).

[26] J.-W. Pan, S. Gasparoni, M. Aspelmeyer, T. Jennewein, and A. Zeilinger, Experimental realization of freely propagating teleported qubits, Nature (London) **421**, 721 (2003).

[27] C. Vitelli, N. Spagnolo, L. Aparo, F. Sciarrino, E. Santamato, and L. Marrucci, Joining the quantum state of two photons into one, Nat. Photon. **7**, 521 (2013).

[28] K. Lemr, A. Černoch, J. Soubusta, K. Kieling, J. Eisert, and M. Dušek, Experimental Implementation of the Optimal Linear-Optical Controlled Phase Gate, Phys. Rev. Lett. **106**, 013602 (2011).

[29] K. Lemr, K. Bartkiewicz, A. Černoch, M. Dušek, and J. Soubusta, Experimental Implementation of Optimal Linear-Optical Controlled-Unitary Gates, Phys. Rev. Lett. **114**, 153602 (2015).

[30] X.-L. Wang, L.-K. Chen, W. Li, H.-L. Huang, C. Liu, C. Chen, Y.-H. Luo, Z.-E. Su, D. Wu, Z.-D. Li, H. Lu, Y. Hu, X. Jiang, C.-Z. Peng, L. Li, N.-L. Liu, Y.-A. Chen, C.-Y. Lu, and J.-W. Pan, Experimental Ten-Photon Entanglement, Phys. Rev. Lett. **117**, 210502 (2016).

[31] G. Brassard, N. Lütkenhaus, T. Mor, and B. C. Sanders, Limitations on Practical Quantum Cryptography, Phys. Rev. Lett. **85**, 1330 (2000).

[32] Y. Zhao, B. Qi, X. Ma, H.-K. Lo, and L. Qian, Experimental Quantum Key Distribution with Decoy States, Phys. Rev. Lett. **96**, 070502 (2006).

[33] Ş. K. Özdemir, K. Bartkiewicz, Y.-X. Liu, and A. Miranowicz, Teleportation of qubit states through dissipative channels: Conditions for surpassing the no-cloning limit, Phys. Rev. A **76**, 042325 (2007).

[34] M. H. Rubin, D. N. Klyshko, Y. H. Shih, and A. V. Sergienko, Theory of two-photon entanglement in type-II optical parametric down-conversion, Phys. Rev. A **50**, 5122 (1994).

[35] S. Popescu, Bell's Inequalities Versus Teleportation: What is Nonlocality? Phys. Rev. Lett. **72**, 797 (1994).